

# BiBlade Sampling Tool Validation for Comet Surface Environments

Paul Backes<sup>1</sup>, Scott Moreland<sup>1</sup>, Fredrik Rehnmark<sup>2</sup>, Mircea Badescu<sup>1</sup>, Kris Zacny<sup>2</sup>, Robert Wei<sup>2</sup>,  
Grayson Adams<sup>2</sup>, Risaku Toda<sup>1</sup>, Peter Vieira<sup>1</sup>, Elizabeth Carey<sup>1</sup>, Robert Krylo<sup>1</sup>, Erik Bailey<sup>1</sup>,  
Carl Seubert<sup>1</sup>, Dylan Conway<sup>1</sup>, Seth Aaron<sup>1</sup>, Harish Manohara<sup>1</sup>,  
Gregory Peters<sup>1</sup>, Marco Mongelli<sup>1</sup>, Dario Riccobono<sup>1</sup>

<sup>1</sup>Jet Propulsion Laboratory  
California Institute of Technology  
4800 Oak Grove Dr.  
Pasadena, CA 91109  
Paul.G.Backes@jpl.nasa.gov

<sup>2</sup>Honeybee Robotics  
398 W. Washington Blvd. #200  
Pasadena CA 91103  
zacny@honeybee.com

*Abstract*—The BiBlade sampling chain was developed for use in a potential Comet Surface Sample Return mission. Following prior versions of the sampling tool, a new tool was developed and validated to TRL 6. Sample acquisition testing was performed across a range of comet simulants and operational conditions. Tool operation was validated in a thermal-vacuum chamber. The end-to-end sampling chain was validated including sampling, sample measurement, and sample transfer. The sampling system is now ready for flight implementation.

## TABLE OF CONTENTS

1. INTRODUCTION.....	1
2. BiBLADE SAMPLING CHAIN CAPABILITIES.....	1
3. SAMPLING CHAIN OVERVIEW .....	2
4. BiBLADE SAMPLING TOOL DESIGN .....	3
5. SAMPLE MEASUREMENT DESIGN.....	9
6. MECHANICAL POROUS AMBIENT COMET SIMULANT .....	10
7. SAMPLE ACQUISITION VALIDATION .....	10
8. OPERATIONAL SAFETY VALIDATION.....	10
9. ENVIRONMENTAL VALIDATION .....	14
10. INTEGRATED TOUCH-AND-GO VALIDATION ...	16
11. SAMPLE MEASUREMENT VALIDATION .....	17

12. END-TO-END SAMPLE CHAIN VALIDATION .....	17
13. FUTURE PLANS.....	18
14. CONCLUSIONS.....	18

## 1. INTRODUCTION

Return of a sample from the surface of a comet was identified as one of NASA’s highest science priorities in the NASA Decadal Survey [1,2]. The BiBlade sample chain was developed to acquire, measure, and store a sample from the surface of a comet in a potential Comet Surface Sample Return (CSSR) mission using a Touch-and-Go (TAG) mission architecture. A previous version of the BiBlade sample chain was built and tested [3]. This paper describes a next generation BiBlade sampling chain and validation testing. This new generation tool improves upon the prior version in various ways including by doubling the sampling energy and by using flight-relevant design rules.

There are various possible mission architectures for a CSSR mission, including lander, harpoon, dart, and TAG [3,4]. The BiBlade sampling chain was developed for use in a TAG mission architecture where a spacecraft would maneuver to several meters from the surface of a small body and deploy a sampling tool at the end of a robotic arm. The spacecraft

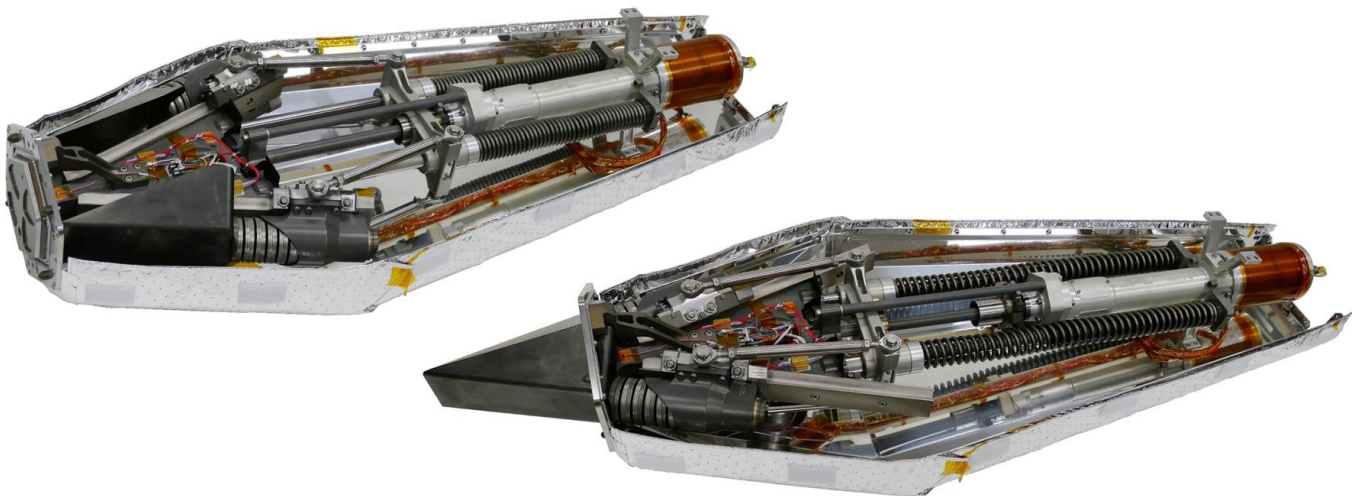


Figure 1. BiBlade sampling tool, open on left, closed on right.

would continue descent to the surface until sample tool contact and then a sample would be quickly acquired and the spacecraft would thrust away from the surface of the small body. The BiBlade concept and several other TAG sampling tools were described and compared in an earlier publication [4]. The BiBlade was selected as the best sampling tool concept due to the unique capabilities it provides with low mission risk. The CSSR mission concept and expected science requirements were described in the Decadal Survey and associated mission study [1,2].

This paper summarizes the capabilities of the BiBlade sample chain and describes the design and validation process used to bring the sample chain to TRL 6. Section 2 lists the capabilities of the sample chain with references to the sections in the paper where the capabilities and validation of the TRL are described. Section 3 provides an overview of the sampling chain, Sections 4-6 describe the design of the sample chain and simulants, Sections 7-12 provide results of validation tests, and Section 13 describes future plans for the sampling chain development. Section 14 summarizes the capabilities of the sampling chain.

## 2. BiBLADE SAMPLING CHAIN CAPABILITIES

The capabilities of the BiBlade sampling chain are listed below, along with the sections in the paper where capabilities and TRL validation are described.

Capability	Section
Acquires comet material with properties from loose regolith to 5MPa cone penetration resistance.	4.2, 7.2
Acquires individual samples up to 500 cc volume.	4.1, 7.2
Acquires subsurface sample.	7.2
Returns two samples from different comet locations.	3, 4.1, 4.4
Enables multiple sampling attempts per sample.	4.1
Survives sampling attempts from any strength comet material.	8.1, 8.2
Preserves sample through benign sampling technique and maintained temperature.	4.1, 4.2, 4.7
Functionality provided with only one actuator and two Frangibolts.	4.1
Prevents anchoring to comet.	4.5
Validated in comet-relevant simulant.	6, 7.2
Tool ready for flight implementation.	4.3, 9
Robust to spacecraft approach conditions.	7.2
Robust to varied surface topographies.	8.2
Safe reaction forces to spacecraft.	8.2, 10

Sampling validated with realistic spacecraft dynamics.	7.1, 7.2
Robust operation in comet environment conditions.	9.1, 9.2
Satisfies contamination control.	4.6
Generates minimal ejecta from surface during sampling operation.	4.8, 7
Robust sample measurement.	5, 11
Robust sample transfer.	4.4, 12

## 3. SAMPLING CHAIN OVERVIEW

The end-to-end sampling chain includes sampling, sample measurement, and sample containerization.

### Sampling

The sampling process begins with the spacecraft several meters from the surface of a comet and the robotic arm with the BiBlade tool at its end deployed to a fixed configuration. The spacecraft then continues its descent until the sampler contacts the surface when the sampling tool would fire, with springs quickly driving two blades into the surface of the comet thereby acquiring and encapsulating the sample, as shown in Figure 2. The spacecraft would immediately thrust away from the surface with the sample in the tool.

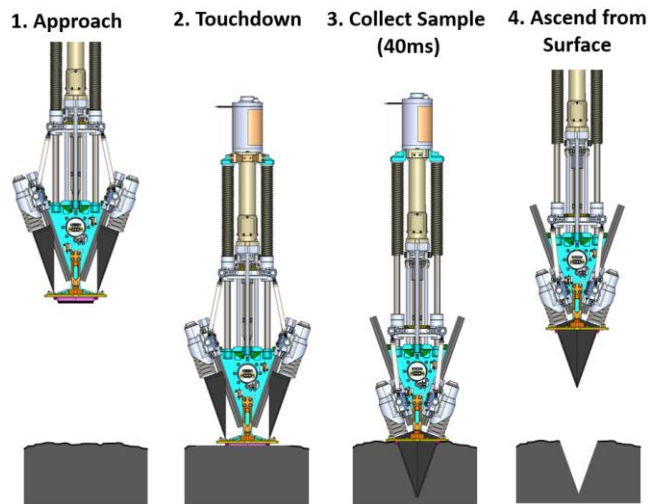


**Figure 2. Touch-and-Go Sampling Sequence**

### Sample Measurement

After the spacecraft has maneuvered away from the surface of the comet, the robotic arm would then transfer the sampling tool to the measurement station and insert the closed blades into the measurement station chamber. The blades would be pulled back slightly to expose the sample in slits between the blades a few mm wide and multiple images



#### 4.2 Design for Sampling

From a fundamental mechanics stand-point, the BiBlade sampler is a high-speed blade penetrator interacting with brittle, porous material. As such, there are a specific set of processes that govern material failure, resistance to penetration and dynamic response. These processes are unique to the family of materials and the regime of penetration speed. Required is the study of applicable penetration mechanics theory, experimentation and modeling for the unique conditions if an efficient design is to be realized. A significant investigation was undertaken at JPL to develop understanding of blade penetration mechanics. Results of the work guided BiBlade penetrator properties such as accelerated mass, velocity, blade geometry and coatings. The penetration theory, experimentation and modeling work can be found in [12].

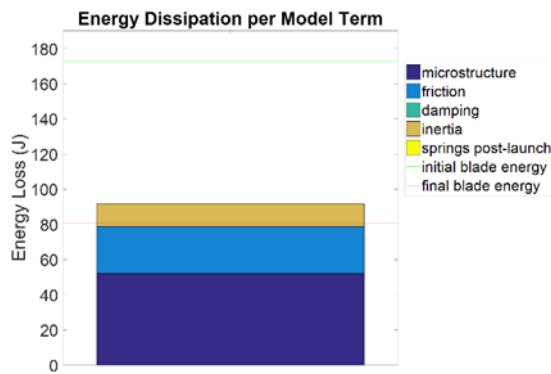


**Figure 5. High-speed blade penetration of 1mm blade with 10m/s initial velocity.**

Penetration resistance (total force required to plunge blade into material) for blade implements in the speed regime of the BiBlade (0-15m/s) has significant contributions from material microstructure strength, inertial resistance (density) and friction against the penetrator wall (see Figure 5). Blade thickness impacts resistance due to both microstructure strength and inertial resistance. A 5% additional dissipation of energy was measured for every 0.1mm of additional blade thickness beyond 1mm. For these reasons the blade thickness was minimized and 1mm wall was implemented. As shown in Figure 5, energy dissipation due to inertial resistance of penetrated material is significant. Maximum penetration velocity was reduced to 10m/s by adding dead-weights to the accelerated bodies. Friction on the blade wall is a significant source of resistance and was studied in depth; including strategies of wide-tip leading edge and low-friction coatings. A low friction coating was implemented as it not only decrease penetration resistance but also decreases retraction/pull-out resistance. A 50% reduction in frictional resistance was realized. Blade tip geometry does not affect penetration resistance. Therefore, it was optimized to engage extremely hard surfaces such as smooth concrete to promote positive engagement (increases system safety, see Sections 4.5, 8.1, 8.2). See [12] for in depth analysis of BiBlade penetrator parameters.

#### 4.3 Mechanism Design and Materials

The BiBlade tool was designed in accordance with NASA and JPL spaceflight hardware standards for motor-driven mechanical assemblies. In a few cases, strategic non-compliant materials and components were accepted in order to accelerate the fabrication schedule and enable early testing. In each case, however, a clear plan to achieve compliance exists and a drop-in flight-like replacement has already been identified (Table 2). The result is a high-fidelity engineering unit that can readily be upgraded with no change to the existing design when increased pedigree is required. The existing BiBlade is designed to withstand a comet sampler mission environmental qualification test program as is, without these upgrades.

**Table 2. BiBlade non-compliances with mitigation plans for flight.**

Item	Non-Compliance (TRL6)	Mitigation Plan (Flight)
Industrial BLDC Motor	Replace bearings and lubricant, add resolver for commutation	Procure custom flight motor with compatible materials
Bearings/Rails	Conventional AISI 52100 bearing steel	Material upgrade to corrosion resistant 440C bearing steel

A partial list of NASA, JPL and aerospace industry standards used in the design of the BiBlade is included in Table 3. Components such as fasteners, bearings and springs were selected in adherence to aerospace industry specifications (e.g., NAS, NA, MS) and procured with material certifications from qualified suppliers. A partial list of flight-like materials used in the TRL6 tool is presented in Table 4.

Since the BiBlade components would be exposed to environments ranging from ambient Earth atmosphere to temperatures as low as -40°C in the vacuum of space, corrosion resistant metals with a low ductile-to-brittle transition temperature were selected. Fasteners with locking features were used to avoid loosening and the resulting loss of preload due to shock experienced when the blades are launched. These features also keep the fasteners from loosening as a result of thermal cycling.

**Table 3. A partial list of NASA, JPL and aerospace industry standards used in design of BiBlade.**

Category	Partial List of Specifications	Applicability (Selected Requirements)
Mechanism Design & Analysis	NASA-STD-5017, NASA-STD-5001B, NASA-TM-106943	Actuator torque margin, structural factors of safety, general design guidelines (fastener retention, redundant springs, etc.), bolted joint analysis
Materials	MIL-HDBK-	Material properties (strength,

	5J, AMS, MSFC-STD-3029	modulus, ductility, thermal expansion, creep, etc.), cryogenic/vacuum compatibility, specifications (materials, coatings, finishes and plating), resistance to stress corrosion cracking
Standard Parts & Fasteners	NAS/NA, MS, SAE AS, ANSI, DIN	Fasteners, nuts, inserts, rod ends, splines, bushings
Electrical	M83513, M22759, M55021	Connectors and wiring
Other		Lubricant, adhesives, paint

Nonmetallic structural materials such as wipers and the cable tray were selected for strength and ductility at low temperature and low outgassing in vacuum to minimize possible contamination of the sample. For the same reason, a minimum amount of low-temperature lubricant (Braycote 601EF) was applied by grease-plating exposed bearing surfaces of the roller screw and any accelerated mechanisms (carriage rollers, slider linear bearings). Sealed bearing surfaces were lubricated more liberally.

Differential thermal growth at critical interfaces was controlled by selecting materials with similar coefficients of thermal expansion (CTE) and by minimizing temperature differences across the body of the tool. Faying aluminum surfaces were chemical conversion coated to ensure good thermal conduction across bolted structural joints. Exposed aluminum surfaces were anodized, partly to provide protection from oxidation but also to promote desired optical properties for efficient radiative heat transfer from the thermal shroud.

**Table 4. A partial list of flight-like materials in BiBlade.**

Item	Materials
Structural members	Aluminum 6061-T6, Ti 6Al-4V
Springs	Ti Beta-C (3-8-6-4-4)
Roller Screw	CX13VD(W) Stainless Steel
Trigger Hooks	MP35N
Release Ring	C95500 bronze
Rod Ends	Inconel 718, 17-4 PH
Fasteners	A-286 CRES
Lubricant	Braycote 601EF
Wipers, Wire Insulation	PTFE
Heaters	Kapton
MLI Blankets	Mylar

#### 4.4 Sample Transfer

Located at the front end of the BiBlade sampler are the sample retaining lids for the SRC vault (Figure 3). Two lids are nested in series and are fixed to a base plate via Frangibolt non-explosive restraints (Figure 6). The Frangibolts are actuated and lid released when the sample is in the SRC vaults. Surrounding the lid baseplate a ring faceplate allows

for thermal shroud mounting, blades guiding and arm shear shunts and guides during sample measurement and sample release. Between the lids baseplate and the ring faceplate a narrow opening is form through which the blades travel for sampling and retrieval. This opening is covered by a set of Teflon brushes to limit the comet material the blades bring inside the tool.

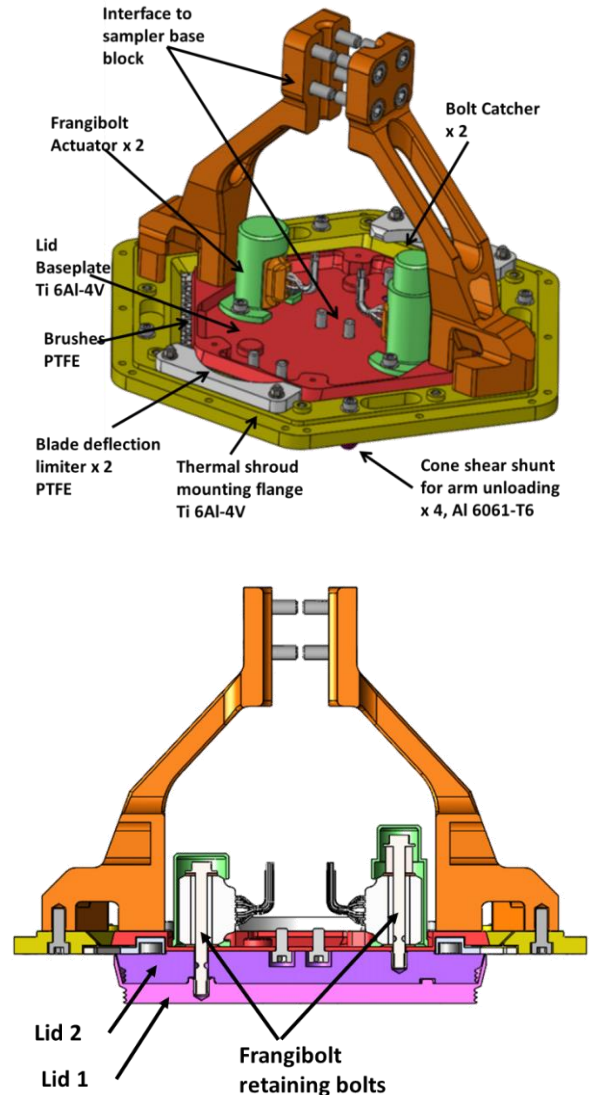


**Figure 6. Lid release assembly components (Top) and cross-section (bottom)**

For sample transfer to the SRC, the arm aligns the tool with an SRC sample vault. The tool inserts the closed blades into the vault pressing and aligning the ring faceplate against the vault front face. Blade tapered faces guide a compliant arm in the transverse direction to align with the vault even with large positioning errors of the arm. After tool mating with the sample vault, the blades are retracted allowing the vault retention spring clips to capture the outermost lid. The cone shear shunts prevent the arm from loading the lids sideways after retrieving the blades in the case of initial misalignment.

With the blades retracted and the lid captured, the corresponding frangibolt is activated, the bolt is broken and the lid is released. A vault dust seal of Nomex felt will prevent fine particles from escaping from the vault. The arm then moves the tool away from the vault.

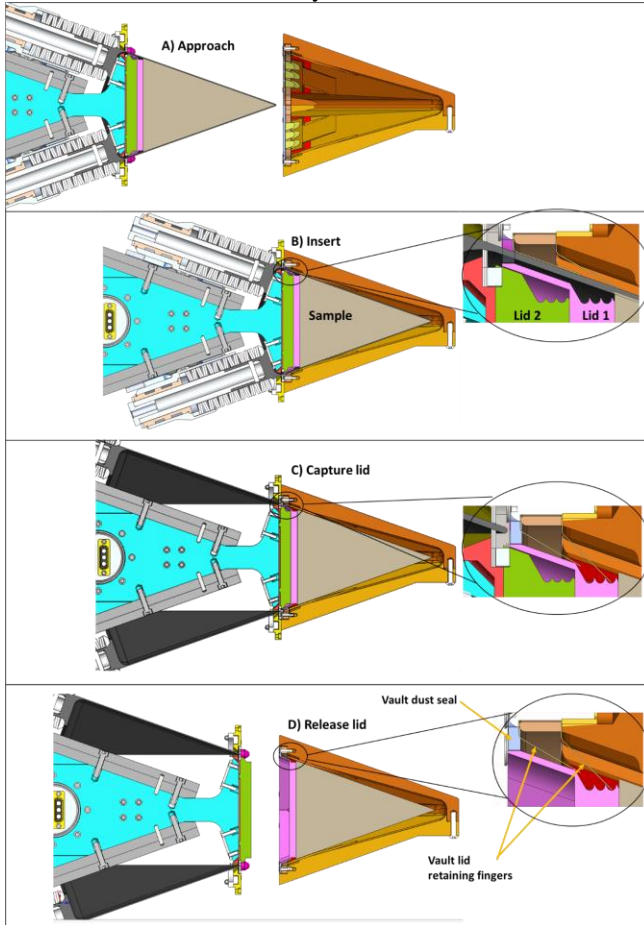


**Figure 7. Sample release procedure: A) The tool with sample inside the close blades approaches the sample vault; B) The tool inserts the closed blades with the sample into the vault and aligns the ring face plate against the vault front; C) The blades are retracted to allow the passive vault retaining fingers to capture the lid; D) The corresponding frangibolt is activated breaking the bolt to release the vault captured lid.**

Two lids allow two samples to be deposited in two different vaults. In the series of pictures shown in Figure 7 both lids are attached to the tool and lid 1 is to be released into the sample vault.

#### 4.5 System Self-safety

The BiBlade sampler has design features to achieve robustness against the following. (1) Hard surface impact damage, (2) Touch-and-Go motion induced forces on the sampler, (3) inducing undesirable loads spacecraft, (4) trapping of blades in comet surface, and (5) dust/debris.

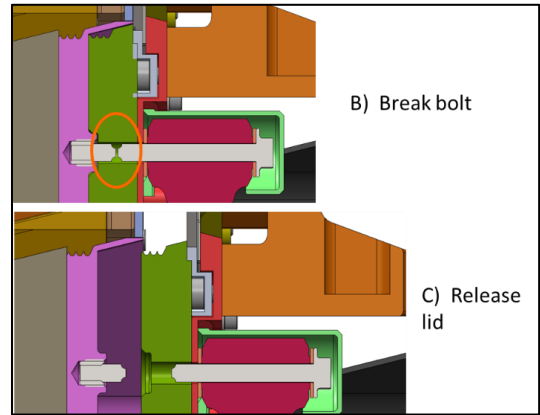


**Figure 8. Lid restraint release details.**

#### Impact Protection Mechanism

The BiBlade is designed to survive firing into vacuum and into perfectly rigid objects.

Figure 9 displays the overload/isolation springs that exist at the base of the blades. All mass other than the blades become sprung and do not encounter significant loads. The overload springs are preloaded to 2.5kN. The two bodies (1. blades, 2. everything else) are intentionally quite different in mass (5.35kg and 0.35kg respectively). Additionally, the overload/isolation spring rate and the blade stiffness are an order of magnitude different. The springs then act as isolators separating the blade body impact and the remaining 5.35kg body impact (Figure 9). Two dynamic events, 2kHz and 0.1kHz occur, therefore the total load is reduced. As the blade body is relatively stiff, a high impact event occurs and dominates compared to the 0.1kHz event. Essentially, the high load impact is solely created by the mass and velocity of the blade (stand-alone body from rest of system). To minimize the peak force, the kinetic energy in the blade body is minimized by limiting the blade velocity and minimizing mass. To do so, a limit of 10m/s of the accelerated bodies is made by adding dead-weight to the roller carriages (not blade body). This results in maximum kinetic energy in the blade (and the 2kHz impact) only being 17.4J (per blade). Compare this value with 265J in the sprung *body*.

When the BiBlade is fired into empty space or there is residual energy after sampling, the same overload spring mechanism strikes a hardstop and arrests motion safely. The load path does not go through the blade body in this case but only through the high-strength base portion of the component.

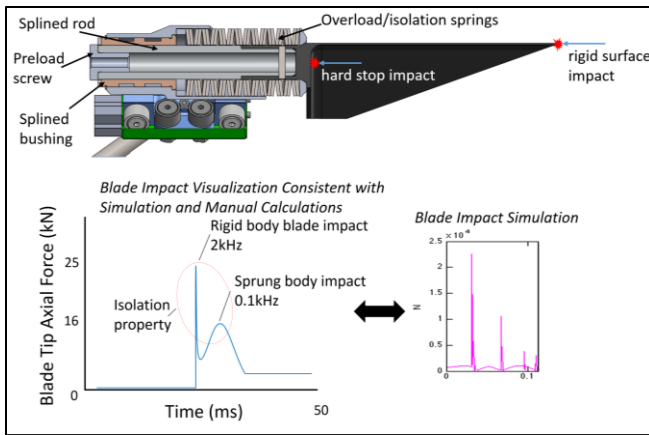


**Figure 9. Design of the blade impact load protection system. A preloaded stack of disk springs (Titanium BetaC) compresses if larger than nominal sampling forces are encountered. It acts to reduce impact forces and isolate blade body impact from sprung body impact loads.**

Static testing of blades (Figure 10) was conducted to verify the buckling mode and critical load for validation of FEA model to be used for static/dynamic analysis. See Section 8.1 for validation of this topic.

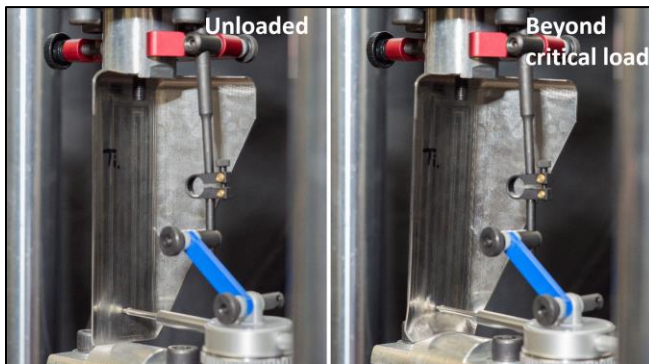


**Figure 10. Static testing of spare blade titanium from TRL5 prototype on Instron machine. A point load at the center of the blade tip induced by an aluminum half-round induced this worst case load condition (buckling).**

### Wrist Spring

A compliant wrist joint is located at the end of the BiBlade as an interface to the robotic arm. This component is made up of a single spring with its long axis oriented collinear to the sampler's long axis. This wrist joint consists solely of a spring with structural flanges on both ends. There are no explicit rotary mechanisms such as bearings or bushings. Note that the Wrist Spring does not deflect in the axial direction (compression direction) but does have angular articulation via bending. The effective spring rate is 2Nm/degree.

The Wrist Spring has two functions. (1) Limit blade moment induced by spacecraft transverse motion, and (2) reduce

spacecraft angular rates induced by the BiBlade when striking an oblique surface.

In Touch-and-Go operations spacecraft lateral motion could exist when the blades are engaging the comet surface. The wrist spring compliance allows lateral motion of the spacecraft without exceeding structural capability of the blades.

The Wrist Spring mitigate the effects of moments imparted to a spacecraft if the blades strike a smooth, rigid surface at an oblique angle. Also, the blade edge would dig into the comet surface to dissipate sampling energy. Multibody simulations of the full sampler-spacecraft system were used to specify spring rate properties and mature the Wrist Spring concept that was eventually validated experimentally (Section 8.2). The Wrist Spring reduces the decoupling of the sampler body and spacecraft body leading to a small fraction of movement being transferred to the spacecraft body, while the blade edge and overload springs positively engage the surface and dissipate large amounts of energy into non-rotating form. See Section 8.2 for validation.

### Robustness to Blade Trapping

Blade geometry and blade pull-back capability prevent anchoring to the comet. The blades are fully tapered in all directions so that the blades release from the comet with any vertical motion. If the blades do not fully close and break off the sample, the actuator has enough torque to exercise an abort procedure to pull back the blades and break the comet material, thus freeing the blades. In an abort procedure, the roller screw nut with the gripper would be driven to grasp the shuttle to pull the blades free from the comet.

In the analysis, the blades are assumed to be partially driven into the comet material and the material exerts both on the inside and the outside of the blades a pressure equal to the compressive strength of the comet material. Twenty percent of the comet material is assumed to be of a sticky nature and needs to be sheared to let go of the blades. A friction coefficient of 0.18 between the DLC (diamond like coating) Ti coated blades and simulant material was determined from testing. When the blades are pulled for extraction, shear forces for 20% of the surface and friction for the rest of the surface prevent the blades from moving. In addition to the force required the blades to extracted, the actuator needs to overcome the drive springs compression as well.

In a parallel development a single blade penetration testbed determined the blade penetration depth as a function of the material strength given a predetermined kinetic energy. Details of the penetration mechanics study can be found in [12]. The penetration depth was used to determine the maximum retraction force (blades extraction plus the drive springs compression) for every material with an unconfined compression strength in the range of 0 to 50MPa. The plot of these max values is shown in Figure 11. A peak value of 8kN retraction force was calculated to be required to extract the blades from the comet material in the assumed conditions and

the actuator was designed to provide this force with design margins.

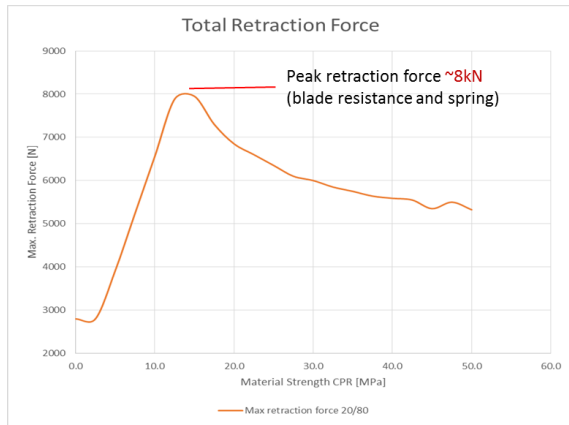


**Figure 11. Total retraction force required.**

#### Dust/debris

The BiBlade was designed to operate robustly in a high dust and debris environment. The thermal shroud acts as a first line of defense and covers the whole sampler other than a 3mm hexagon slot at the front end of the sampler where blades pass through. This slot is protected by three layers of PTFE seals (Figure 12) that wipe the blades, and prevent material from entering when interacting with the comet surface. In addition to the PTFE seals, rigid break-off features exist if particles are strongly adhered to the blades (i.e. knock off large particles). As a back up to the wiper/breakers, all exposed mechanisms are tolerant of operating in an environment with hard particles up to 1.5mm (gripper/release mechanism is an example). Meanwhile, the large diameter carriage rollers are capable of crushing all simulants tested if particles this size are present on the rails. All other components have seals and/or wipers.

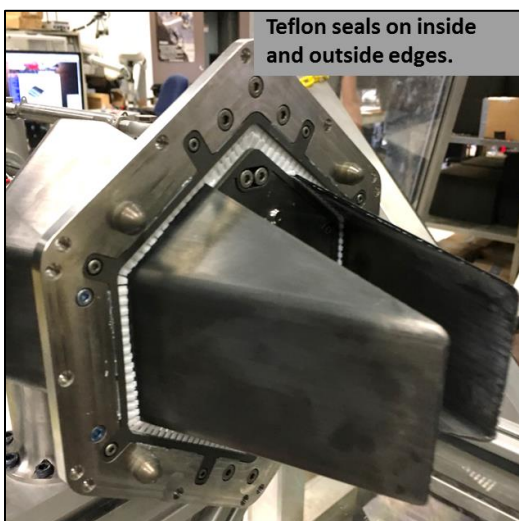


**Figure 12. Close-up of dust/debris seals that wipe blades and close off only opening not covered by debris/thermal shroud.**

#### 4.6 Contamination Control

The BiBlade was designed to be compliant with contamination control requirements that would be needed for a CSSR mission. The following strategy was implemented for the BiBlade prototype: select compliant materials where possible, contain non-compliant materials, and bound maximum ppm of non-compliant material. There are two primary sources of contamination, Braycote 601 EF lubricant and the sampling blade coating. All remaining materials of the BiBlade were considered compliant materials as reviewed by JPL scientists.

Braycote lubricant was minimized by using a 90%-10% grease plating process. This deposits a very thin coating of lubricant via evaporation process, thus minimizing total contaminant volume (weighing parts before/after process measured total mass). Grease plating also achieves high adhesion thus reducing migration.

Conventional bearings were grease plated (this using minimal contaminant) and sealed. Braycote located in accelerated/decelerated components was also in the grease plate form but contained via enclosures and ballistic shields. Together, minimization via grease plating, implementation of enclosures and ballistic shields provided an approach consistent with JPL contamination control methods. See Figure 13 for diagram of accelerated body ballistic shields.

The blade coating was considered a possible contaminant but deemed compliant as total mass possible to get into the sample is low. The diamond-like carbon coating (hydrogenated amorphous carbon a-C:H) was acceptable as manufactures adhesion tests and BiBlade testing showed it doesn't wear or flake off. Bounds for coating contaminant level (assuming 1% of coating will fall into a 500cc sample) would be 2.4ppm by volume. This was confirmed an acceptable value.

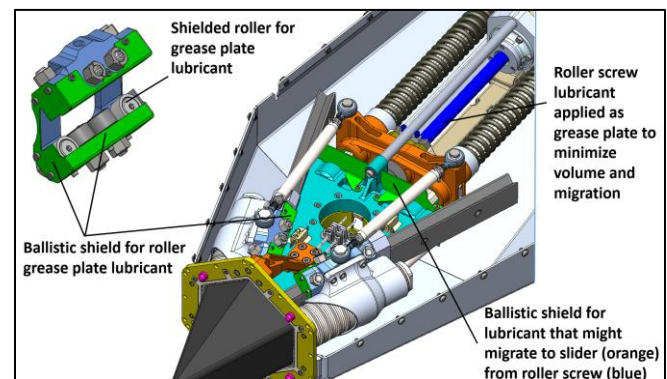


**Figure 13. Implementation of shielding as part of the contamination control strategy for lubricants. Large decelerations can act to fling lubricant however multiple layers of shielding (including ballistic) employed to minimize contamination.**

#### 4.7 Thermal Control

The BiBlade was designed to operate in the thermal environment expected to be found at a comet located 4-5AU. For design requirements, this is a 70K black body sink with no solar flux (all exposed surface low absorptivity). The thermal control system was designed to keep all sampler components within their allowable flight temperatures and maintain surfaces contacting the sample below  $-25^{\circ}\text{C}$  as to not cause alteration (science requirement). The design was specified for steady state and transient heating operations (motor usage). The primary thermal control components were.

- Rigid aluminum thermal shroud with mirror-like internal finish
- 15-layer MLI blanket shroud cover
- Two heating circuits with Honeywell 706S-27A-14 preset thermostats, film motor heater and base block power resistors (as heaters)
- High thermal resistance structural interface to wrist-joint/robotic arm

See Figure 14 annotation for more detail. All thermal control components were flight components drawn from JPL flight inventory.

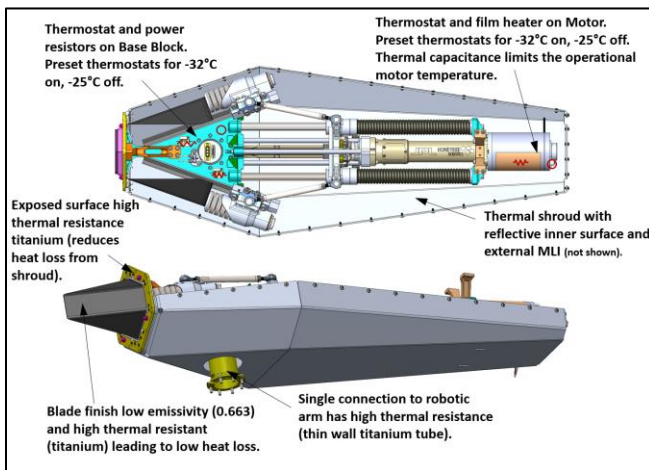


**Figure 14. Diagram of thermal control system elements implemented and validated in BiBlade prototype.**

FEA thermal modeling of the BiBlade was conducted prior final construction of the sampler. Critical bodies and interfaces were modeled including (Figure 15), heated/temperature controlled motor, heated/temperature controlled base block (primary structure), blade interface, blade, rigid aluminum shroud, shroud MLI (blanket insulation), and the robotic arm interface. The model was configured to analyze heated element power requirements and allowable flight temperatures for critical bodies (including blade maximum temperature).

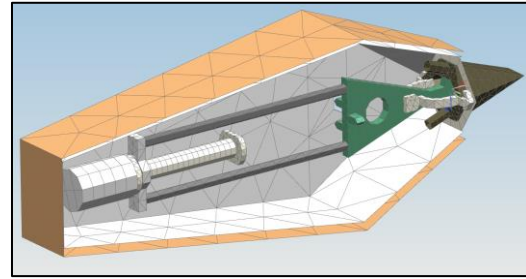


**Figure 15. FEA thermal model of BiBlade sampler.**

The model shows blade can be maintained below  $-25^{\circ}\text{C}$  with large margin (to prevent sample alteration), while allowable flight temperatures of components met. See Figure 16 for results. The thermal control system was validated during a full sampling system thermal-vacuum test with background temperature of  $-160^{\circ}\text{C}$  as described in sections 9.1 and 9.2 for thermal-vacuum test validation.

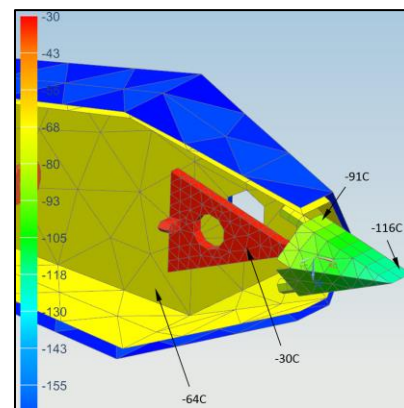


**Figure 16. Thermal model results of steady state condition.**

#### 4.8 Minimization of Ejecta

Minimization of ejecta caused by sampling is important to limit the amount of ejecta that could transfer to spacecraft surfaces. Two primary design features minimize ejecta generated during the sampling process. First, use of thin blades for penetration minimizes the energy imparted during the sampling process. Second, during the approximately 40ms of the sampling process the forward momentum of the blades causes the tool body to slightly recoil away from the comet rather than move into the comet.

### 5. SAMPLE MEASUREMENT DESIGN

The Fiberscope Sample Imaging (FiSI) system was developed to provide sample measurement for the BiBlade sampler [5]. A FiSI chamber would be mounted on the spacecraft and nine fiberscopes would be arranged in the walls of the chamber, as shown in Figure 17. The robotic arm would insert the blades of the BiBlade sampling tool into the FiSI chamber, as shown in Figure 18. The blades would be pulled back slightly to expose the sample through slits a few mm wide. The fiberscopes would passively transfer views of

the surface of the sample to a common camera which would acquire one picture that includes images from all of the fiberscope locations. Each imaging fiberscope consists of approximately 30,000 silica-based picture elements. At the distal end of each fiberscope a gradient-index (GRIN) cylindrical objective lens is attached to focus the image onto the fiberscope. The fiberscopes would be combined in a bundle that could enable the camera to be placed in a warmed volume in the spacecraft while the distal ends are in the more extreme space environment.

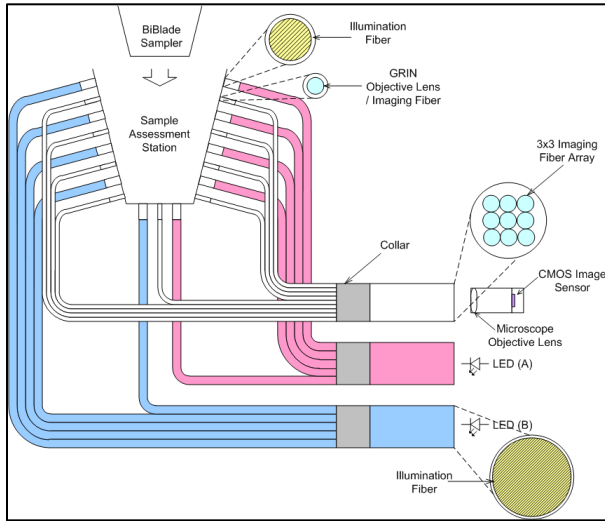


**Figure 17. Fiberscope Sample Imaging System Design.**

The sample would be illuminated by light sources mounted next to the fiberscopes in the sample measurement chamber. The light sources would be in two groups, one group for each side of the chamber. One light emitting diode (LED) would generate light into the fibers that carry the light sources for each group. The purpose of having two light source groups is so that the sample measurement system can be used in two modes: 1) imaging the sample, and 2) a through-sensor. When imaging the sample, both light groups are turned on and then nine images are acquired of the sample. When using FiSI as a through-sensor, only one group of lights is turned on and then the images are acquired. In this case, if a light is seen by a fiberscope, then there is no sample between it and the light source on the opposite side of the chamber.

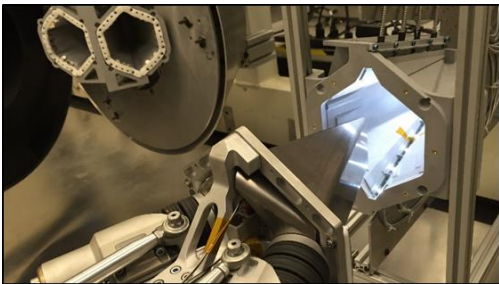


**Figure 18. Inserting blades into FiSI chamber.**

The configuration of the light sources was selected so that the sample measurement would be robust to dust collecting on the windows in front of the fiberscope imagers. With the light sources to the side of the imagers, the light path is from a light source, into the chamber, reflected off the sample and then into the imaging fiber. Dust on a window could degrade an image, but there would still be an image. This feature was confirmed in the tests described in Section 11. The through-sensor configuration was designed so that the sample measurement would be robust no matter how much dust accumulated on the windows in front of the imaging fiberscopes, as was also confirmed through testing.

## 6. MECHANICAL POROUS AMBIENT COMET SIMULANT

A suite of simulants were developed to represent a range of potential comet properties. A mix design called Mechanical Porous Ambient Comet Simulant (MPACS), as shown in Figure 19 was developed using Portland cement and pumicite combined and added to water and a foaming agent. Strength properties were varied by changing the amount of foaming agent added to the mixture. The MPACS material was fabricated into 8-inch cubic boxes for the BiBlade test program. Density, cone penetration resistance (CPR), uniaxial compressive strength (UCS), shear strength, and porosity were measured.



**Figure 19. Mechanical Porous Ambient Comet Simulant (MPACS) simulant block.**

## 7. SAMPLE ACQUISITION VALIDATION

The validation of BiBlade sample acquisition performance was conducted utilizing a testbed designed to account for interface and operational scenarios, and a suite of simulants including in-house manufactured and material used by other agencies for prior missions [6].

Validation of BiBlade sample acquisition confirmed

- Collection of sample volumes of 250cc to 500cc with at least 75cc below 4cm of the surface
- Capture of material up to a strength of 5MPa cone penetration resistance (CPR) of relevant simulant - MPACS
- Robustness to local surface slope angle
- Compatibility with interfaces and full-system properties including stiffness and spacecraft inertias
- Robust to approach velocities up to combined 4cm/s axial

and 4cm/s transverse

- Clean capture to enable Touch-and-Go ascent operation of spacecraft (pull-out force <25N, full blade closure)

The Sample Acquisition System Testbed (Figure 20) was used for most of the BiBlade tests. Key attributes of the testbed are; (1) linear actuator to representing spacecraft approach velocity (any angle), (2) planar representation of antenna spring pivot interface, (3) representation of full spacecraft inertia via flywheel geared to 2200kg, (4) simulant surface orientation adjustability.

Due to space limitations of the publication, only results of the enveloping test configuration are presented. These represent worst-case operational scenarios and act as conservative results when reporting BiBlade capabilities.

The test configuration was as follows

- Sample Acquisition System Testbed
- 5.7cm/s approach velocity at 45° (equivalent to 4cm/s axial and 4cm/s transverse)
- 2Nm/degree antenna spring
- 2.5-5MPa CPR MPACS, 0.5 CPR Foamglas T4, 3.9MPa CPR Foamglas HLB1600 (“F”)

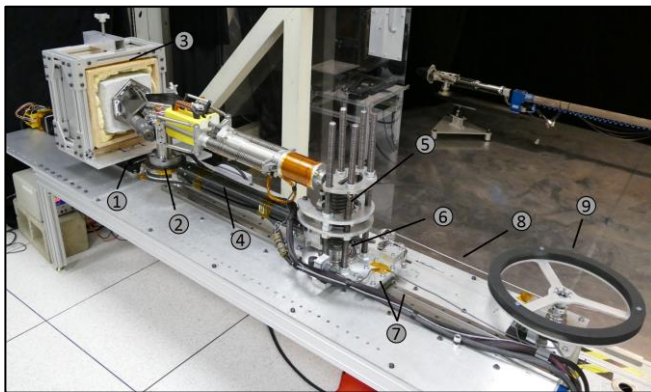


Figure 20. Sample Acquisition System Testbed utilized for validation and characterization of sampling performance. Critical parts consist of (1) “approach velocity” linear stage with adjustable pointing direction, (2) force/torque sensor, (3) simulant fixture, (4) sampler/space-craft connecting tube, (5) tunable spring loaded pivot (represents Wrist Spring), (6) pivot cross-roller bearing, (7) ball bearing carriage (2x) and rail for axial motion, (8) cable for load transfer to flywheel, (9) flywheel representing 2200kg S/C inertia, \*not visible are four position sensors.

Results of the sample acquisition tests are plotted in Figure 21. The blade end of travel penetration rate (blade velocity) and sample volume acquired are metrics used to determine capability. The results of two pass fail metrics were also recorded but not displayed since all test results were positive for the range of strength. Failures were only observed above 5.6MPa CPR, however graceful degradation occurred. These metrics were (1) blade full closure and (2) pull-out force

978-1-5090-1613-6/17/\$31.00 ©2017 IEEE

<25N. The latter would be equivalent to a maximum thruster force a spacecraft might have to ascend from the surface.

The BiBlade can successfully acquire MPACS of 4MPa CPR while collecting half volume capacity of the blades (250cc) and collect 75cc below 4cm from the surface. 75cc below 4cm from the surface is equivalent to a 250cc total sample, which leads to using 250cc as a benchmark. At this material strength, the blades still maintain an end of travel speed of 2-3m/s (initial speed 10m/s).

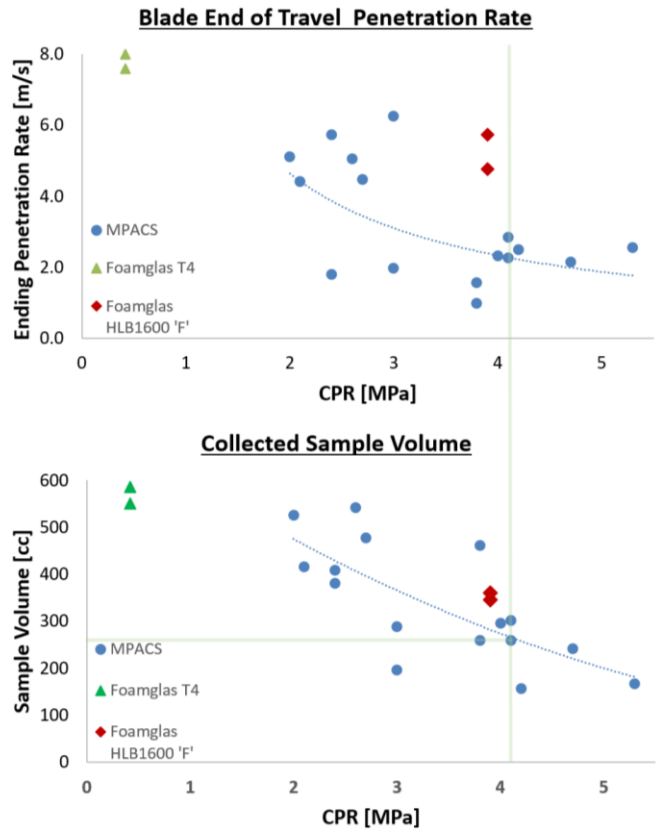
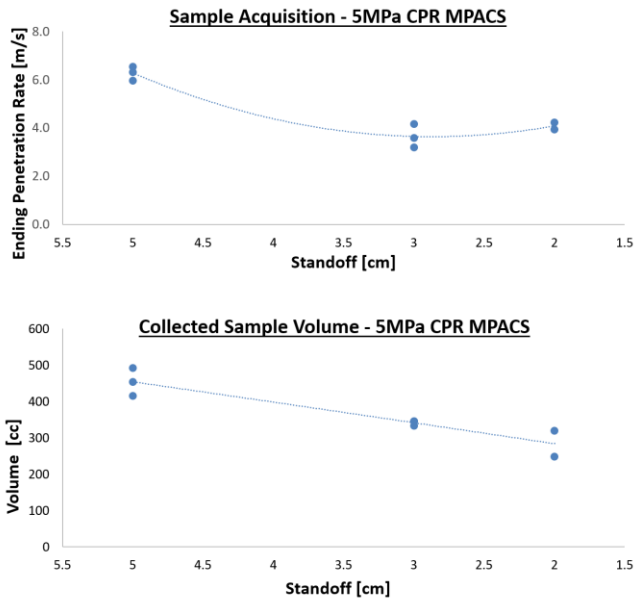


Figure 21. Sampling validation results from Sample Acquisition System Testbed. Configuration for all tests were with touchdown velocities of 4cm/s axial and 4cm/s transverse combined and tool perpendicular to simulant surface. This configuration is representative of the most difficult scenario with respect to other touchdown velocities and surface topologies.

Weak top layers material such as dust are possible with strong material present below them on comet surfaces. Tests strictly investigating the capability of sampling MPACS of 5-6MPa CPR (binned as 5MPa) included an approximation of the effect of a dust layer over the stronger material. Little energy is expended on the weaker upper layer, therefore larger sample volumes or stronger sub-layers can be acquired. The dust layer was represented by a stand-off from the material surface. Figure 22 displays the test results approximating the effect of a dust layer. Results show the capability of the BiBlade to acquire 300cc of material with as little as 2cm of dust and 450cc of material with 5cm of dust.



**Figure 22. Sample Acquisition System Testbed results with dust layer simulated as standoff from surface. With as little as 2cm dust (i.e. weak material), the BiBlade can collect 250cc to 450cc of 5MPa CPR MPACS.**

The Sample Acquisition System Testbed was deemed overly conservative when reporting BiBlade performance. This is due to excessive deflections of low stiffness components such as the fly wheel cable. Although efforts to increase rigidity where made, highspeed camera analysis shows total deflections greater than 2cm for 4-5MPa CPR simulants. The BiBlade would be expected to have higher sampling capability when mounted to a system with more direct load path to the 2200kg mass. As such, a full-scale spacecraft testbed is being constructed (Figure 40) at JPL to support higher fidelity testing of the BiBlade sampler.

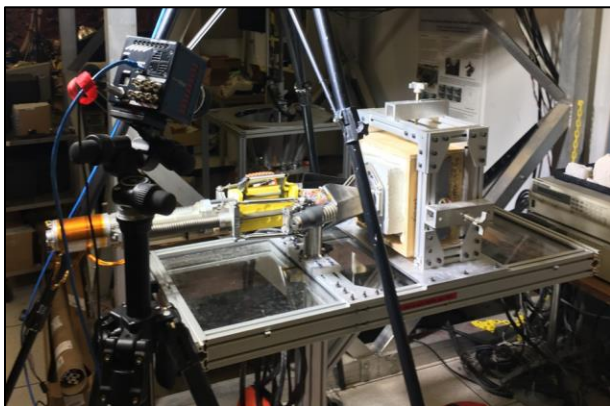


**Figure 23. BiBlade sample acquisition testing with Rigid Testbed. Both the sampler base and simulant block are rigidly fixed. In this configuration the BiBlade was shown to reliably sample 5.0+MPa CPR MPACS simulant but an upper limit of 7MPa was demonstrated.**

The Rigid Testbed was used to evaluate the BiBlade when  
978-1-5090-1613-6/17/\$31.00 ©2017 IEEE

both the sampler and simulant block are fixed (Figure 23). In this configuration, the BiBlade reliably sampled 520cc volumes of 5MPa CPR MPACS simulant (Figure 24).



**Figure 24. Shown is an acquired sample of a 5.2MPa CPR MPACS simulant block from the Rigid Testbed. The hole created reached 15cm depth and acquired a mostly intact 520cc volume sample. The blade end of travel velocity was 5.5m/s (at full blade closure). Four tests ranging from 5.2 to 5.6 MPa CPR were repeated with similar results.**

A test was performed to acquire fly ash to validate acquisition of weak material and to assess the generation of ejecta during sampling, as shown in Figure 25. The prior version of the BiBlade was used, but the blade speed was the same as for the current BiBlade. Fly ash is an unconsolidated and fluffy material with negligible strength.



**Figure 25. Sampling fly ash.**

The test validated that the BiBlade fully acquires very weak material. The picture in Figure 25 is from the moment when the maximum amount of ejecta can be seen. It shows a small amount of ejecta, but it is believed that the primary cause of the ejecta was disturbance of the fly ash from the air that was pushed forward by the blades' motion. A better test for ejecta generation would be done in a vacuum chamber to eliminate the effect of air movement and at micro-gravity so gravity does not affect the ejecta motion. These tests are being considered for follow-on work.

The BiBlade sample acquisition capabilities have been verified to meet the following attributes.

- Collection of sample volumes of 250cc to 500cc with at least 75cc below 4cm of the surface
- Capture of material of strength 0-5MPa cone penetration

resistance (CPR) of relevant simulant - MPACS

- Compatibility with Touch-and-Go like operations with full-system properties including spacecraft inertias and velocities (4cm/s axial and 4cm/s transverse )
- Clean capture to enable ascent operation of spacecraft (pull-out force <25N, full blade closure)

## 8. SAMPLE TRANSFER VALIDATION

The sample transfer testbed consists of a robotic arm, the BiBlade and the SRC vaults (Figure 26). Mechanical compliance of the robotic arm and tapered blades allow the sampler blades to act as large alignment features enabling robust insertion into the SRC vault and attachment of the lid.

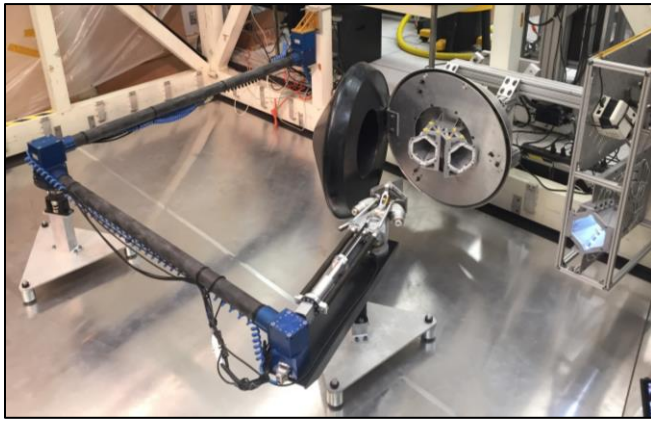


**Figure 26. Validation of sample transfer using high fidelity testbed. Includes weight off-loaded 3-DoF robotic arm of representative stiffness, BiBlade with Frangibolt actuator lid restraint, sample measurement/verification station and SRC geometric mock-up with two sample vaults.**

There were four aspects characterized and/or validated during the testing:

- Use of Frangibolt non-explosive actuators for lid restraint (shock considerations)
- Opening & re-closing blades in measurement station
- Translational/rotational initial misalignments
- Hard inclusions and protrusions between blades

To verify that the opening and re-closing of the blades for sample measurement does not affect sample transfer, each of the following tests included the opening/closing process to mimic sample measurement. Additionally, Frangibolt actuation (non-explosive bolt breaker) was included in each test to verify shock induced does not affect lid capture.

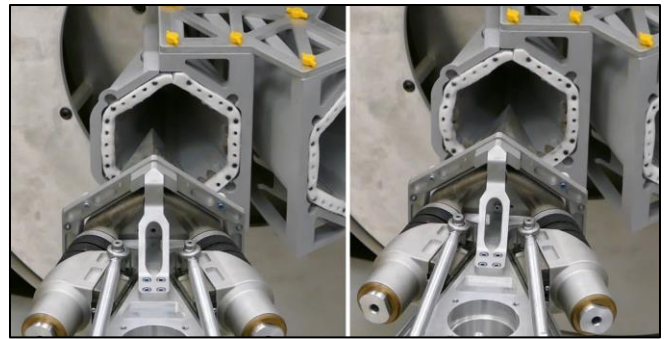


**Figure 27. Validation of robustness to robotic arm misalignment during insertion of BiBlade into SRC vault. Linear and angular offsets were introduced and proper lid deployment and capture was verified. A 4cm transverse offset (left figure) and 5° angular offset (right figure) are shown to have no adverse effects on sample transfer.**

To validate robustness to robotic arm positional error, axial and transverse offset were introduced and angular offset were introduced (Figure 27). It was verified that 4cm transverse/axial misalignment and 5° angular misalignment with the SRC do not prevent the sample from being successfully transferred to the SRC vaults and the lid fully engaging the locking features.

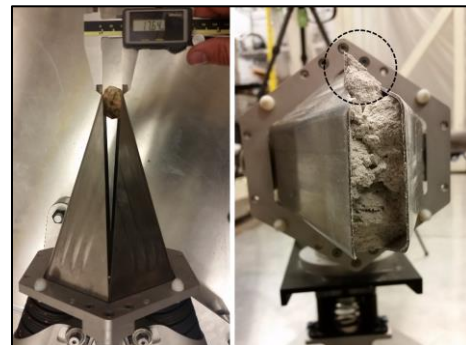


**Figure 28. Validation of sample transfer/containerizing robustness to large inclusion between blade edges creating gap or deflection and protrusions. Rocks (left figure) and comet simulant protruding shards (right figure) were intentionally placed between blades. Scenarios shown successfully transferred to the sample vault.**

Robustness to hard inclusions stuck between the blade edges and sample material protrusions was verified (Figure 28). Rocks up to 2cm in diameter were placed between the blades. Rigid protrusions were created by sampling MPACS simulant of 9MPa cone penetration resistance and shards manually orient to protrude from the blade. Robustness to these scenarios were designed into the SRC vaults via special geometry.

Summary of successful sample transfer validation with the following attributes:

- 3DoF planar robotic arm with relevant stiffness and open-loop position control
- Use of Frangibolt non-explosive actuators for lid restraint (shock considerations)
- Opening & re-closing blades for measurement
- Translational/rotational initial misalignments up to 4cm axial and transverse misalignment, 5° angular misalignment
- Hard inclusions between blade edges of 2cm and protrusions between blades up to 4cm
- Lid locking features

An example of a transferred sample and close up of the SRC geometric mock-up is provided in Figure 29.

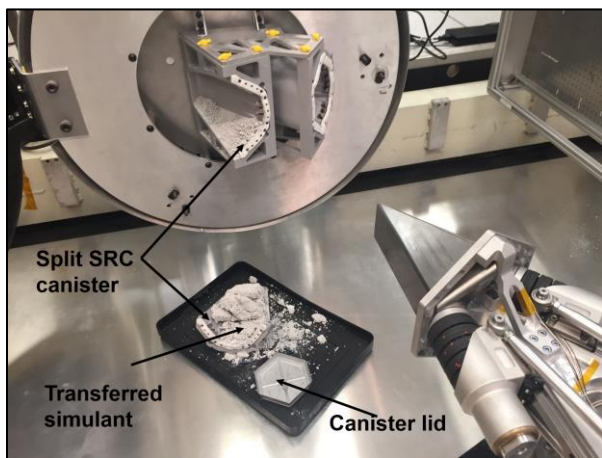


**Figure 29. Example of transferred sample manually removed from SRC vault. Sample vault splits in half to disengage lid locking features.**

## 8. OPERATIONAL SAFETY VALIDATION

The BiBlade is designed to self-protect against damage to itself and the spacecraft. The primary features to do so are (1) the blade impact overload/isolation mechanism, (2) the Wrist Spring and (3) blade pull-out/abort capability via high torque actuation and low resistance coating blades. This section provides validation of the blade impact protection and spacecraft load transfer reduction.

### 8.1 Self-safety Results

The structural integrity of the blades and function of the impact overload/isolation mechanism was verified via full system testing of the BiBlade while striking a high rigidity object. The blades and the overload/isolation mechanism are designed to prevent damage to all parts of the BiBlade when striking a perfectly rigid surface at maximum blade velocity. Maximum velocity is reached when there is 15cm stand-off between the BiBlade front plate and the surface of the struck object.

As a worst-case interaction, the tests were configured so only one blade strikes the test surface. This imparts almost the full 300J of the sampler through a single blade load path. The

surface struck was a concrete cinder block. The relatively smooth cinder block selected was considered by Icy Body scientists to be highly conservative with respect to surface smoothness's that could potentially exist on a comet. Figure 30 shows a test at the moment of the blade impact. Post-test visual inspection showed no damage to the blade or any component of the sampler. These tests validated the feature of the sampler that it may strike a surface of any hardness and not lead to self-damage.

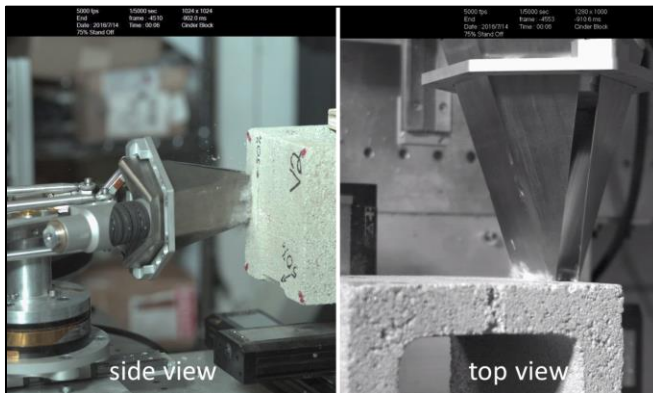


**Figure 30. High speed video frames of blade survivability verification during impact. The worst case scenario was configured consisting of a high stiffness material (cinder block), maximum stand-off (highest kinetic energy in blades) and single blade interaction. Only starboard blade hits block. The overload/isolation mechanism successfully prevents damage to the blades.**

### 8.2 Oblique Strike Results

Striking of a smooth, rigid surface at an oblique angle could impart significant side loads to the blades and a moment about the spacecraft. Two aspects of the BiBlade design are intended to alleviate this potential issue. These are the Wrist Spring and the anchoring effect that the blade edges create when striking even a sloped surface.

A planar (2-D) representation of the Wrist Spring was created for the Sample Acquisition Systems Testbed. This consisted of a pair of counter loaded torsion springs and a cross-roller bearing that was capable of being reconfigured with different spring rates and preload. A planar implementation was used since the Wrist Spring would not support testing in 1-g.

Multibody simulations of the full sampler-spacecraft system were used to select the spring rate to evaluate. A spring of 2Nm/degree was selected. A Wrist Spring of equivalent rate was fabricated so it could be used in the off-loaded full-scale testbed. The sampler-spacecraft full system simulation also indicated that a 45-degree surface angle is of worst case. Figure 31 shows the testbed configured for the oblique strike scenario validation.



**Figure 31. Validation testing of energy transferred to S/C during rigid surface oblique strike scenario. Shown is a rigid, smooth surface (cinder block) fixed at 45° to the BiBlade sampling axis with the face of the sampler touching. This configuration represents the worst-case scenario for blade interaction with a surface that may lead to excessive spacecraft rotational rate.**

The BiBlade fired into the 45° cinder block four times to validate blade survivability and measure energy that would be transferred to the spacecraft via moment transfer that would contribute to angular rate, with results shown in Figure 32. Validation of the structural integrity of the blade was confirmed via visual inspection. Only minor scratching in the form of <1mm yielding occurred on the blade tip.



**Figure 32. Inspection post-test of the oblique strike scenario shows that the blades are undamaged. The point of the blade tip promotes positive engagement of the smooth cinder block surface.**

The rotational energy of the BiBlade pivoting about the torsion springs was measured to evaluate energy that may be transferred to the spacecraft leading to angular rates. The energy was measured two different ways. First by measuring the angular rate of the BiBlade with no torsion springs attached and the second method was to measure the energy stored in spring compression (i.e. maximum angle of rotation). It was determined that most energy was lost during the surface impact interaction (high frequency vibration of components, cinder block chipping and overload spring compression). Table 5 lists the energies calculated for each oblique strike test. Typical values of energy transferred to the rotation system were under 6J while the last test was 19J due to significant blade sliding. This was due to the blade edge being sanded down during multiple tests, therefore not able to positively engage the cinder block surface.

**Table 5. Rigid, smooth surface oblique strike test results measuring the dynamic response as rotational energy that could be transferred to spacecraft.**

Test	Maximum Angular Rate of Sampler [deg./s]	Maximum Spring Deflection [deg.]	Energy via Initial Angular Rate [J]	Energy via max. Torsion Spring Compression [J]	Pushback Force X, Y [kN]
1 – no spring	52	N/A	6	N/A	2, 0.7*
2 – w/ spring	34	4.4	3	4	-
3 – w/ spring	75	4.7	12	5	2, 0.7*
4 – w/ spring, blade slid	115	14.7	28	19	2, 0.7*

\*  $\tan^{-1}(2/0.7) = 19\text{deg}$  (blade angle)

Results indicate that <<10% of the sampler’s compressed spring energy is transferred to the BiBlade-Wrist Spring system. For a 5500kg\*m<sup>2</sup> spacecraft the rotational rate would be 5.8 degrees/s assuming 100% momentum transfer. However, applying simple moment/energy transfer equations yields only 1/16<sup>th</sup> the energy of the BiBlade-Wrist Spring pivot system would be transferred to the spacecraft. Therefore the expected maximum angular rate of the spacecraft due to oblique strike of a smooth, rigid object is 1.4 degrees/s. This result validates the ability of the sampling system to protect the spacecraft from BiBlade induced angular rates in even highly conservative worst-case scenarios.

## 9. ENVIRONMENTAL VALIDATION

The BiBlade was designed to operate in thermal and pressure environments expected at comets up to 5AU from Earth as well as near earth thermal loading. Thermal-vacuum testing was conducted to validate the environmental design aspects and to quantify system performance in a flight-like environment (Figure 33). A custom cold-shroud of much smaller size than the vacuum chamber was constructed to achieve very cold temperatures by reducing the thermal mass required to cool and by minimizing radiative losses. A slot allowed for high speed video (5000fps) of the blade motion. The number of thermal cycles of the test is consistent with design practices for the type of hardware and orbital profile of a comet mission.

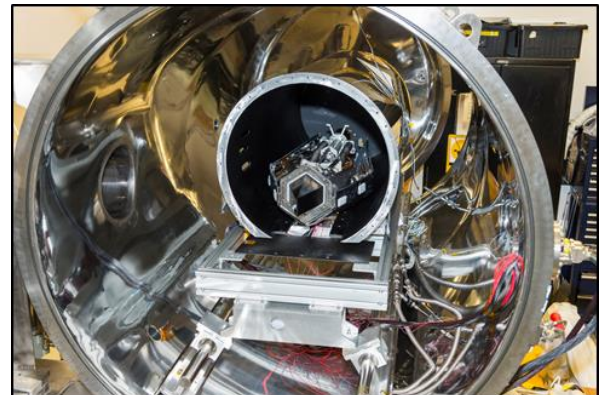


**Figure 33. Environmental testing of BiBlade in thermal-vacuum chamber. Cold shroud end plate and top half of BiBlade thermal/dust shroud removed for photo.**

Thermal-vacuum test configuration:

- Cycling between +70°C and -160°C (three cycles)
  - High power AC heaters on sampler to bring sampler internal temperature to +70°C
  - Cold shroud avg. temperature -160°C (measured by four thermocouples)
  - Sampler thermal control system maintained internal temperature during cold phase between. Thermostat set points were -32°C to -25°C
- Pressure  $10^{-7}$  torr (high vacuum)
- Functional testing
  - Perform actuator homing operations at each cold cycle
  - Functional test at last cold phase consisting of self-fire sampling operations five times
- Performance verification
  - Verify thermocouples read values within allowable flight temperatures of the components
  - Verify surfaces contacting sample (blades) do not exceed -25°C
  - Verify that actuator maintains adequate torque/current margin
  - Verify kinetic energy available for sampling (blade speed) within 5% of Standard Temperature/Pressure condition

### 9.2 Thermal-Vacuum Test Results

The sampling system - actuator and mechanisms - and thermal control system functioned as design during all aspects of the thermal-vacuum tests.

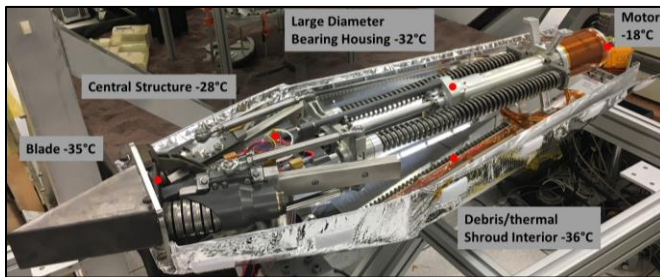


**Figure 34. Temperature of critical components during cold/vacuum operation testing with -160°C cold shroud. Measured temperatures (see red dots for locations) were consistent with component allowable temperature limits and requirement of sampling surfaces (blade) to maintain temperature below -25°C.**

The thermal control system maintained components within their specified allowable flight temperatures; including observing the -25°C blade upper limit with a 10°C margin. Figure 34 provides temperature measurement of critical locations within the BiBlade. Once the internal temperature of the sampler reached steady state, the blades were retracted to firing position, held in this position for five minutes and then temperatures recorded. The blade retraction hold is a required operation that inadvertently raises the temperature of the blades slightly due to retracting into the sampler debris/thermal shroud.

978-1-5090-1613-6/17/\$31.00 ©2017 IEEE

Although the BiBlade mechanisms were designed for the environmental conditions of the thermal-vacuum test, design validation and quantification of degradation due to expected temperature effects was completed. The sampling system was evaluated in two parts, (1) The actuator and roller screw mechanisms related to blade retraction (compressing the firing springs) and (2) The accelerated bodies, blades and associated mechanisms that store kinetic energy during the sampling penetration process. Table 6 reports the blade end of travel speed and the actuator torque/current margins for standard temperature/pressure and at the thermal-vacuum, test cold conditions.

The blade speed metric represents kinetic energy available in the blade for sampling. The test results (Table 6) show little degradation in potential sampling ability while functioning in the -160°C/ $10^{-7}$  torr environment. An average loss of speed and kinetic energy was only 1% and 2.5% respectively. A minimum actuator torque/current margin of 181% was recorded therefore exceeding the 150% margin requirement. Although the torque/current margin of the actuator was much less than at standard temperature/pressure, this was expected when operating Braycote lubricant in the -40°C range.

**Table 6. Environmental validation functional test results. Energy transfer to blade and actuator torque/current margin are metrics in cold/vacuum conditions.**

	Standard Temperature/Pressure	Environmental Conditions, -160C/ $10^{-7}$ torr	
Blade End of Travel Speed [m/s]			
	10.43	9.68	9.87
	9.80	9.47	9.73
	9.87	9.37	9.81
	9.68	9.64	9.73
	9.47	9.52	9.03
	9.37	9.78	9.35
	9.64	10.63	9.28
average	9.75	9.66	
st. dev.	0.34	0.40	
Actuator Torque/Current Margin [%]			
	500	181	
	429	200	
		200	
average	465	194	
st. dev.	49.9	10.8	

## 10. INTEGRATED TOUCH-AND-GO VALIDATION

The autonomous, closed-loop, thruster-controlled Formation Control Testbed (FCT) [7,8] was used to demonstrate sampling of a representative comet surface for a TAG Concept of Operations as shown in Figure 35. The integrated robotic spacecraft with attached BiBlade tool floated on air bearings and autonomously performed the integrated proximity operations and sampling. The tests used the JPL Lander Vision System (LVS) [8,9,10] with the Minimal State Augmentation Algorithm for Vision-Based Navigation

(MAVeN) algorithm[7] for terrain-relative sensing and state estimation.

Demonstrations with the sampling tool on the FCT robot showed repeatable performance of the autonomous trigger to detect surface contact without a dedicated sensor, instead using post-contact control error signal buildup compared against a threshold of position error. It was shown that the sampling force to cut and sample the simulant imparted a disturbance onto the thruster-controlled robot that was easily within the authority of the 1-lb thrusters and attitude/flight-path control algorithms. The only appreciable dynamic disturbances were when the sample was not penetrable by the tool, but the dynamics imparted upon the 450 kg robot was still within reasonable dynamic limits for the autonomous control system to arrest the imparted Delta-V, equivalent to 6 cm/s on a full-scale CONOPS spacecraft of 2200 kg.

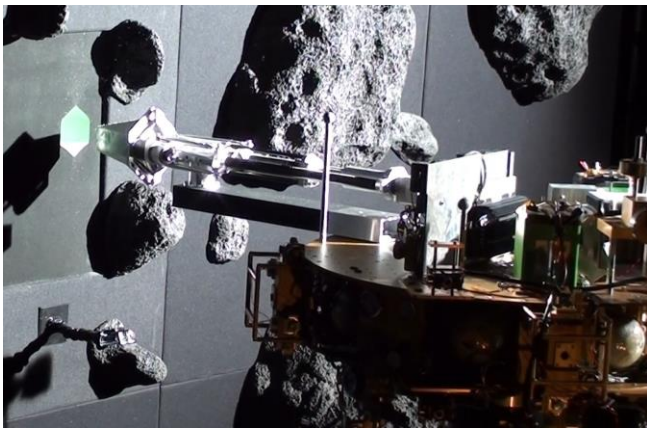


**Figure 35. Integrated proximity operations and sampling. BiBlade was mounted on an air-levitated spacecraft emulator and automated Tough-and-Go approach and sampling was demonstrated using flight-like controls.**

### 11. SAMPLE MEASUREMENT VALIDATION

Four validation tests were performed, 1) measurement in end-end-to-end testbed, 2) fiberscope cryogenic test 3) fiberscope environmental test, and 4) window dust.

A complete FiSI sampling system with nine fiberscopes was built and integrated into the End-to-end testbed. The FiSI system is shown in Figure 18 and the End-to-end testbed is shown in Figure 38. Images of the sample were acquired as expected. A test was performed to demonstrate the FiSI system robustness to cryogenic temperatures. A GRIN lens was attached to a fiberscope imaging fiber (with 30,000 elements) using cryo-grade adhesive. The fiber with GRIN lens was then dipped in LN2 (-196°C) and then 70°C water alternatively for five cycles. Images were taken of a pattern during the testing with minimal degradation. The image during the fifth cycle is shown in Figure 36 This test demonstrates that the FiSI system will not need heaters for the flight implementation.

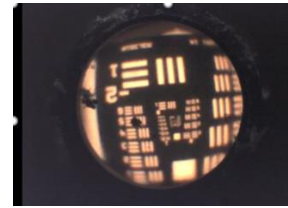


**Figure 36. FiSi Fiberscope image during cryogenic test.**

An environmental test was performed on a FiSI fiberscope where the distal end was placed in environmental chamber (Bemco FTU1.8-100x600) while the image was periodically collected by optics and CMOS camera placed outside of the chamber. The environmental chamber was filled with nitrogen gas at atmospheric pressure. The fiberscope successfully survived five temperature cycles between -170°C and 70°C. The fiberscope image resolution before and after this environmental test was essentially unchanged.

An experiment was performed where a large amount of MPACS dust was placed on the windows over the fiberscopes. Figure 37 shows the resulting images for cases where there is sample in front of the fiberscopes and when there is no sample in front of the fiberscopes. As expected, the dust degrades the image of the sample, but the sample can still be seen in the image. Where there is no sample, the system works well as a through sensor in the presence of dust on the fiberscope windows since the light sources on the opposite sides of the chamber can be seen.

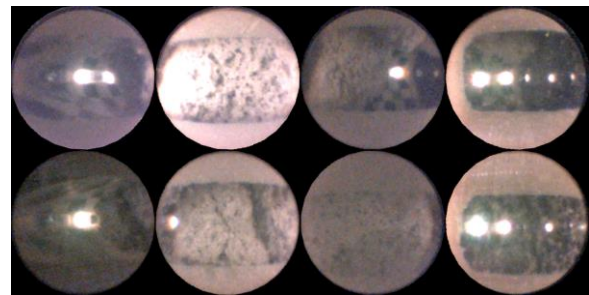


**Figure 37. Fiberscope images with dust on the windows.**

### 12. END-TO-END SAMPLE CHAIN VALIDATION

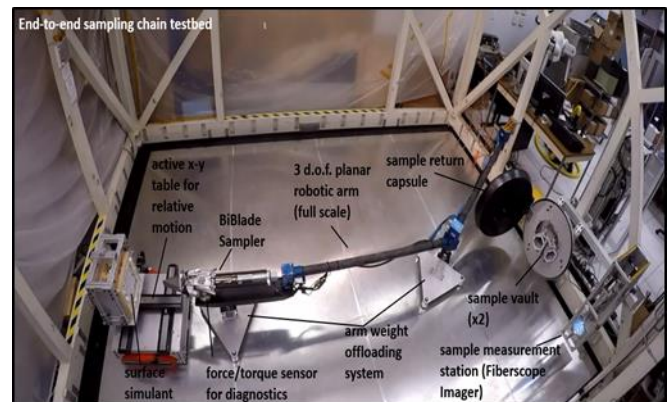


**Figure 38. End-to-end sampling chain testbed.**

The end-to-end sample chain was validated with the prior version of the BiBlade sampling tool and reported in [3]. The validation tests were performed in the End-to-end testbed shown in Figure 38. The end-to-end validation steps are shown in Figure 39. A full-scale robotic arm deployed the BiBlade sampling tool to a fixed position. An X-Y table moved the MPACS comet simulant to the tool and upon contact the tool fired to acquire the sample. The arm moved the tool to the FiSI sample measurement station where the sample was measured, and then the sample was deposited in a sample chamber in the Sample Return Capsule mock-up.

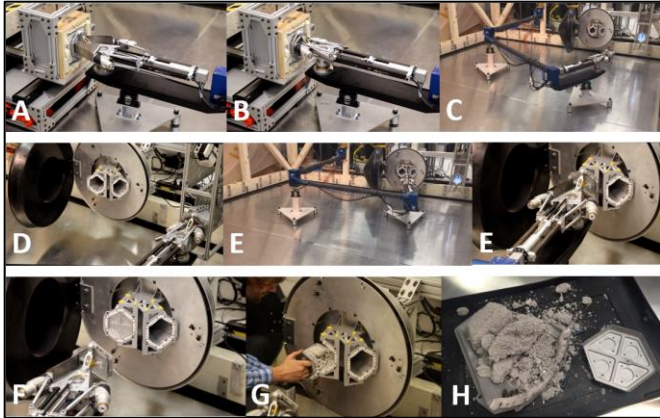


**Figure 39. End-to-end sample chain test sequence. (A) Simulant block approaches. (B) Sampler blades triggered and rapidly close (~40ms) for sampling. (C) Robotic arm retracts and inserts BiBlade into Sample Measurement Station. (D) Sample measurement via fiberscope images. (E) Robotic arm inserts BiBlade into an SRC vault. (E) Blades retract leaving sample in vault and Frangibolt releases lid to seal sample. (F) BiBlade moves away from SRC. (G) Opening of sample vault to show acquired sample. (H) Full sample of MPACS simulant displayed.**

### 13. FUTURE PLANS

#### 13.1 Full-scale Testbed

A full-scale testbed is being fabricated to enable end-to-end validation of Touch-and-Go (TAG) sampling, sample measurement, and sample transfer to a Sample Return Capsule (SRC). Each of these capabilities has been validated but using several testbeds. This testbed will enable end-to-end validation in one testbed. The spacecraft emulator will have representative spacecraft weight of about 2200 kg and will float on air bearings. Initially the testbed will be used for TAG sampling validation over various approach conditions and simulant strengths. For these initial tests, the tool will be mounted directly to the spacecraft structure in a way that is representative of the mounting stiffness for the mission, as shown in Figure 40. A robotic arm will be added to hold the sampling tool and TAG sampling tests will be repeated. The sample measurement system and SRC will be added to the spacecraft and then the end-to-end sampling chain will be validated.

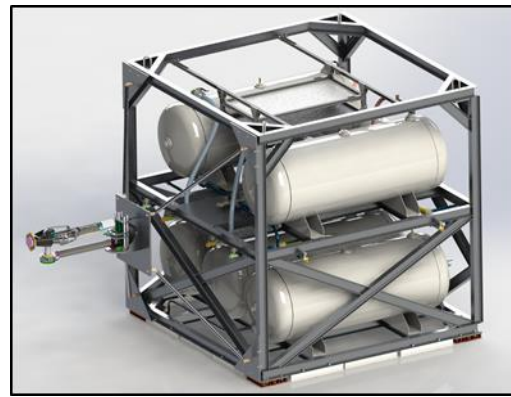


**Figure 40. Full-scale air-levitated spacecraft emulator (2200 kg) is being constructed for integrated validation of Touch-and-Go dynamic sampling, sample measurement, and sample transfer to SRC under various operational conditions. This CAD representation shows the initial configuration for sampling – the robotic arm, sample measurement station, and SRC will be added for end-to-end validation testing.**

#### 13.2 Ejecta Testing

The results of the ejecta test shown in Figure 25 were affected, and potentially dominated, by air motion. Future tests to validate that minimum amount of ejecta is generated during sampling are planned to be conducted in a vacuum chamber to eliminate the effect of air motion.

## 14. CONCLUSIONS

The BiBlade sample chain was developed and validated to TRL 6. The tool was designed with flight design rules and cases of flight-non-compliance were documented and flight implementation options were described. The next version of the tool can be an engineering model for a mission.

The BiBlade has many capabilities and features that make it a desirable tool for a Comet Surface Sample Return mission, while having a relatively simple mechanical design with only one actuator and two Frangibolts. A list of some of the capabilities and features are provided in section 2. The tool enables return of two samples from different locations on a comet, including subsurface samples. Use of thin blades that are driven into the comet surface enables minimized effect on the sample. The tool can acquire samples over a wide range of mechanical properties and survives off-nominal operational conditions.

## ACKNOWLEDGEMENTS

The research described in this publication was carried out at the Jet Propulsion Laboratory, California Institute of Technology, under a contract with the National Aeronautics and Space Administration (NASA).

## REFERENCES

- [1] Vision and Voyages for Planetary Science in the Decade 2013-2022, Committee on the Planetary Science Decadal Survey, National Research Council, The National Academies Press, 2011.
- [2] G. H. Fountain, et al., "Comet Surface Sample Mission Study", SDO-11998, prepared for NASA's Planetary Science Division, April 30, 2008.
- [3] P.B. Backes, et. al, "Experimental Results with the BiBlade Sampling Chain for Comet Surface Sampling," IEEE Aerospace Conference, March 5-12, 2016, Big Sky, Montana.
- [4] P. Backes, et. al., "Sampling System Concepts for a Touch-and-Go Architecture Comet Surface Sample Return Mission," AIAA Space, 4-7 August 2014, San Diego, California
- [5] R. Toda, et al., "FiSI: Fiberscope Sample Imaging System for Robotic Comet Surface Sample Return Missions," 2016 IEEE Aerospace Conference, March 5-12, 2016, Big Sky, Montana.
- [6] T. Spohn, et al., "Thermal and mechanical properties of the near-surface layers of comet 67P/Churyumov-Gerasimenko," *Science*, vol. 349, no. 6247, 2015.
- [7] Scharf, Keim, and Hadaegh, "Flight-Like Ground Demonstrations of Precision Maneuvers for Spacecraft Formations—Part I and II", IEEE SYSTEMS JOURNAL, VOL. 4, NO. 1, MARCH 2010
- [8] Johnson et. al., "Design and Ground Test Results for the Lander Vision System", AAS 13-042
- [9] Johnson, Chang, Montgomery, Trawny, Tweddle, and Zheng, "Real-Time Terrain Relative Navigation Test Results from a Relevant Environment for Mars Landing", AIAA SciTech 2015
- [10] Johnson , Aaron, Chang, Cheng, Montgomery, Mohan, Schroeder, Tweddle, Trawny, and Zheng, "The Lander Vision System for Mars 2020 Entry Descent and Landing", AAS Rocky Mountain Section Guidance, Navigation, and Control Conference, 2017.
- [11] NASA New Technology Report (NTR) #50296
- [12] Moreland, Diaz Lankenau, De Candido, Badescu, Backes "Penetration Mechanics Modeling & Validation of Blade Implements into Porous, Brittle Comet Simulant", IEEE Aerospace Conference, March 4-11, 2017, Big Sky, Montana.

## BIOGRAPHY



**Paul Backes, Ph.D.** is the Group Supervisor of the Robotic Manipulation and Sampling group at JPL. He received BSME degree at U.C. Berkeley in 1982 and Ph.D. in ME from Purdue University in 1987. He received the 2004 NASA Software of the Year Award, 2008 IEEE Robotics and Automation Award, and 2014 NASA Exceptional Service Award.



**Scott Moreland, Ph.D.** received the B.S. degree from University of Toronto and M.S. and Ph.D. degrees in Mechanical Engineering from Carnegie Mellon University and joined JPL in 2013. His expertise is primarily in design and validation of robotic systems that interact with the ground for mobility or sampling.



**Fredrik Rehnmark** is a senior systems engineer at Honeybee Robotics. He received his Master of Science in Mechanical Engineering degree from University of California at Berkeley.



**Mircea Badescu, Ph.D.** is a Technologist in the NDEAA lab at JPL. He joined JPL in 2005 after serving as a Caltech Postdoctoral Scholar. He received the Ph.D. degree in robotics in mechanical and aerospace engineering, from Rutgers University, in 2003. His primary expertise is in design and validation of planetary sampling systems and ultrasonic piezoelectric devices.



**Kris Zacny, Ph.D.** is Vice President and Director of Exploration Technology Group at Honeybee Robotics. His interests include robotic drilling, excavation, sample handling and processing, and geotechnical systems. He previously managed numerous mining projects in South African mines. He received his Ph.D. at U.C. Berkeley in Mars drilling and ME in Petroleum Engineering. Dr. Zacny has over 100 publications, including an edited book titled "Drilling in Extreme Environments: Penetration and Sampling on Earth and Other Planets".



**Robert Wei** is a Project Engineer at Honeybee Robotics. He received a Bachelor's degree and a Master of Engineering degree in Mechanical Engineering from Cornell University. His graduate work focused on controls and dynamics in robotic systems.



**Grayson Adams** joined Honeybee Robotics in the fall of 2015 where he works as a Mechanical Engineer on unique sampling and drilling systems. He received his B.S degree in mechanical engineering from the University of Southern California, where he is also currently pursuing an M.S. in Mechanical Engineering.



**Risaku Toda, Ph.D.** received a B.S. degree in Applied Physics and a Ph.D. degree in mechatronics and precision engineering from Tohoku University, Sendai Japan. He also received a M.S. degree in materials science and engineering from University of

California Los Angeles. Since 2003, he has been with Nano and Micro Systems group at JPL. His research interests include fabrication of MEMS sensors, actuators and nanotechnology devices for aerospace applications. He holds several US patents.



**Peter Vieira** joined the Robotic Manipulation and Sampling group at JPL in August 2014. He received his Master of Science in Electrical & Computer Engineering at Georgia Institute of Technology. The focus of his Masters was robotics software and control systems. At JPL he develops controls and autonomy for planetary manipulation and sampling systems.



**Elizabeth Carey** is a member of the Planetary Ices group at Jet Propulsion Laboratory. She joined JPL in 2013 after receiving a B.S. degree in Astrophysics and a Master of Science degree in Physics from California State University, Northridge. She is the Research Lead of the Geo Analogs task for Mars 2020 and participates in experiments studying the thermal and mechanical properties of ices.



**Robert Krylo, P.E.**, is a mechanical engineer with 38 years of thermal control experience in the aerospace industry. At JPL he has worked on a variety of systems including a methane heat pipe for an interferometer, a single-phase Freon loop for a Mars lander, a suspended, low mass heater for highly stable mirror control, thermal control systems for Earth-orbiting radiometers, and a passive thermal control system for a Mars spectrometer. Robert has a M.S. in Engineering degree from California Polytechnic University, Pomona.



Erik Bailey



Carl Seubert



**Dylan Conway** is a PhD student in Aerospace Engineering at Texas A&M University's Land, Air, and Space Robotics Lab. His research focus is on estimation, computational vision, and navigation. He is a NASA Space Technology Research Fellow and has a BSME from University at Buffalo.



Seth Aaron



**Harish Manohara, Ph.D.** received the Bachelor of Engineering degree in instrumentation technology from the Bangalore University, India in 1989, followed by an M.S. degree in nuclear engineering in 1992, and a Ph.D. degree in engineering science in 1997 from the Louisiana State University, Baton Rouge, Louisiana. In 1998, he became an Assistant Professor of Research at the Center for Advanced Microstructures and Devices (CAMD) at the Louisiana State University. In November of 2000 he joined JPL to develop advanced silicon and vacuum electronic devices for THz applications. Since 2005, he has been leading the Nano and Micro Systems (NAMS) group at JPL and has developed carbon nanotube field emitters, nanoelectronic devices, miniature spectroscopic instruments, and MEMS for space, defense, medical, and commercial applications.



**Gregory H. Peters** is a member of the Geophysics and Planetary Geosciences Section at the Jet Propulsion Laboratory. Currently he is a Surface Sampling and Science (SSS) Scientist for the Mars Science Laboratory mission and the Cognizant Engineer of the Geo-Analogs task for the Mars2020 Mission. He joined JPL in 2001.



**Marco Mongelli** received the Bachelor of Engineering degree in Mechanical Engineering from the Politecnico di Torino, Italy, followed by a M.S. degree both Mechanical and Mechatronic Engineering Master's Degrees as a result of the partnership between the Polytechnic of Turin and the University of Illinois at Chicago.



**Dario Riccobono** received the B.S. degree from Politecnico di Torino (Italy), where he is currently pursuing an M.S. in Aerospace and Astronautic Engineering. He is working at JPL on the control system for a full scale spacecraft emulator for a potential comet sample return mission.

